Brillouin scattering of semicrystalline poly(4-methyl-1-pentene): study of surface effects of bulk and film material

J. Krüger and L. Peetz
Fachrichtung 11.2 Experimentalphysik, Universität des Saarlandes, Bau 22, D-6600 Saarbrücken, W. Germany
and M. Pietralla
Abteilung Experimentelle Physik I, Universität Ulm, Oberer Eselsberg, D-7900 Ulm, W. Germany

Partially crystalline but highly transparent poly(4-methyl-1-pentene) has been investigated as bulk and film material by Brillouin scattering. Special surface effects have been demonstrated in terms of elastic compressional and shear constants. The temperature dependence of the hypersonic velocity has been studied between 17 and 350K indicating a glass transition temperature of 288K.

INTRODUCTION

Poly(4-methyl-1-pentene)* (P4MP1) has the outstanding feature of high optical transparency (comparable to PMMA) in spite of its crystallinity. This is due to the fact that the densities of the crystalline and amorphous phases match at about 323K, the density of the crystalline being even lower than that of the amorphous part at lower temperatures. Moreover, the birefringence of the spherulites vanishes at that temperature[1] and seems to be only slightly affected by temperature.

Thus measurements of Brillouin scattering (BS) are possible in bulk material, which in the case of other semicrystalline polymers are restricted to thin films or backscattering due to the very strong elastic scattering. These measurements have been reported recently[2-5]. It was shown that the use of multipass spectrometers permits BS of amorphous and crystalline polymer films of about 100 μm thickness[4]. As will be shown below we were able to study the elastic behaviour of polymer films in arbitrary directions relative to the film, down to a film thickness of about 18 μm[3].

The observed sound velocities show a surprising dependence of anisotropy. It seems reasonable to correlate such behaviour with special surface effects which should become increasingly dominant with decreasing film thickness. To elucidate this point, bulk material and typical surface structures will be investigated separately. We have investigated the surface of injection-moulded samples which are known to have such typical structure. In contrast to the bulk, quasi transverse and transverse phonons could be detected only in the surface regions. These are the only transverse phonons which we have observed in a polymer by BS transverse phonons have been already reported by Patterson[4].

We have also studied the dispersion behaviour of annealed P4MP1 bulk material. We found no dispersion down to 17K. From measurements between 190 and 309K we further conclude that the change of the refractive index as a function of temperature is smaller than 10^{-4} K^{-1}. Some of the above conclusions were only possible by making a special choice of scattering geometry, eliminating the influence of the fractive index.

* P4MP1 (trade name TPX) was kindly supplied by Mitsui Petrochemical Industry Ltd, Japan

SAMPLE CHARACTERIZATION

Since most properties of polymers vary with sample processing, samples were characterized by d.s.c. and X-ray measurements. The glass transition temperature, the temperature of the melt-peak maximum and the crystallinity are listed in *Table 1*. The injection-moulding yields the highest crystallinity (see sample 2) in good agreement with X-ray measurements on similarly processed samples[7]. Determination of crystallinity by X-ray techniques was not possible due to orientation in some of the samples.

The chill-rolled films are of lower crystallinity with a lower melting point than bulk samples. In addition, the glass transition temperature increases with this higher cooling rate, which is effectively enhanced with decreasing sample thickness on account of heat conduction effects.

The glass transition temperatures determined by d.s.c. coincide with reported values[8].

In view of the discrepancy between the glass transition temperatures reported in the literature and those from BS measurements (*Figure 9*) we have repeated the d.s.c. investigations with lower heating rates of 10 and 5 k/min giving T_g = 304 and 308K, respectively. A further heating rate of 2.5K/min gave no peaks. There is no clear dependence of T_g on the heating rate in d.s.c. however, it seems that the change of thermodynamic parameters, such as temperature are the main contribution to this discrepancy.

The manufacturer claims the film to be free of orientation. We have proved this by means of X-ray wide-angle scattering and birefringence measurements. We confirmed the 200 μm film to be free of orientation using these two methods (in the plane of the film). The thinner films are of increasingly planar orientation (see *Figure 1*). This may be

0032-3861/78/121397-08$02.00

Table 1 Sample characterization

Sample No.	Sample dimensions (mm^3)	Processing	Glass transition[a] region (K)	Melting peak[a] temperature [K]	Crystallinity[a,b]
1	15 x 10 x 3	Injection-moulded annealed 3 h 353K	–	–	–
2	15 x 10 x 3	Injection-moulded	313–317	509	0.32
3	15 x 10 x 3	Injection-moulded			
4	15 x 10 x 0.2	Chill-rolled[e]	315–317	505	0.24
5	15 x 10 x 0.1	Chill-rolled[e]	316- 320	505	0.23
6	15 x 10 x 0.05	Chill-rolled[e]	– [d]	505	0.24
7	15 x 10 x 0.018	Chill-rolled[e]	– [d]	505	0.27
8	10 x 10 x 10	Cut from rod of 70 mm ϕ, annealed 24 h at 423K as already reported		509	0.32

[a] Measured using a Perkin–Elmer DSC-2, heating rate 20 K/min; [b] with 118.2 J/g as heat of fusion[6]; [c] the molecular weight distribution has been determined by gel permeation chromatography, resulting in $M_w/M_n = 1.80$; [d] could not be determined for technical reasons; [e] die temperature 573K, chill-roll temperature, 298K

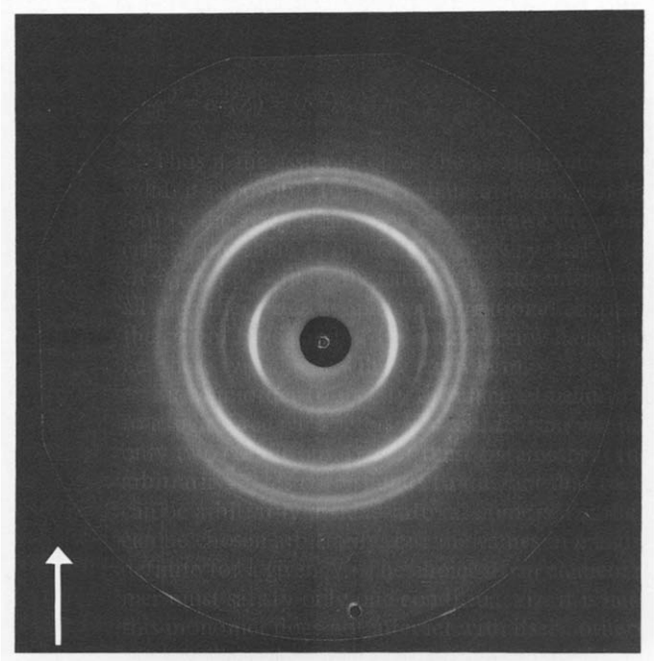

Figure 1 Wide-angle X-ray scattering (plane film) of the 18 μm film Roll direction indicated by arrow

due to a layer of trans-crystallization at the film surface.

The refractive index has been determined at $T = 298.5$K with an Abbé refractometer (Zeiss: Model A) and laser light sources.

λ_ω[nm]	$n^{298.5}$
514.5	1.4672
632.8	1.4617

EXPERIMENTAL

Figure 2 shows the Brillouin scattering set-up used for the measurements. The Fabry–Pérot is a piezoelectric scanning triplepass apparatus (FP1). Piezoelectric scanning Fabry–Pérot apparati generally work in a non-linear fashion (~5%). The degree of non-linearity has been determined by comparing measurements on quartz, glass (BK-7), benzene, cumol and methanol at fixed temperature, made using a *linear* pressure scanning Fabry–Pérot FP2[9] with readings obtained from the *non-linear* FP1. It was found that a polynomial of

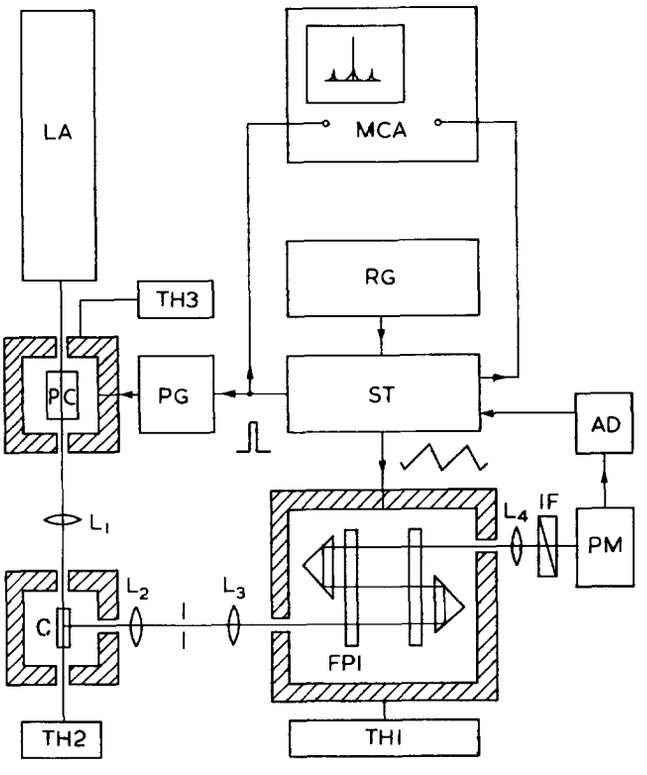

Figure 2 Finesse- and cavity stabilized Brillouin set-up. LA, Laser; PC, Pockels cell; TH 1,2, 3 thermostats; PG, pulse generator; L1, 2, 3, 4, lenses; C, cryostat, MCA, multichannel analyser; RG, ramp generator; ST, Fabry–Pérot stabilizing system; FP1, triplepass Fabry–Pérot; IF, interference filter; PM, photomultiplier; AD, amplifier–discriminator

second order was sufficient to reduce the non-linearity of the linearized spectra to below 0.5%. However, the linearity of every measured spectrum was controlled and any hypersonic frequency given below is an average of the equivalent hypersonic frequencies of two spectral orders.

Even very transparent polymers sometimes show intolerable elastic scattering. The overloading of the photomultiplier by the 'central' line due to elastic scattering was eliminated by modulation with a Pockels cell (PC).

The periodic modulation pulse train consists of 3 pulses of different duration, which are generated by 4 monostable multivibrators IC1–IC4 (*Figure 3*). The MCA start pulse (*Figure 3*) triggers the monoflops IC1, 2 and 4 with the time constants T_2, T_2 and T_4. Monoflop IC3 is triggered by the output pulse of monoflop IC2. The outputs of the monoflops are composed by the nand-IC5 to the resulting signal Q

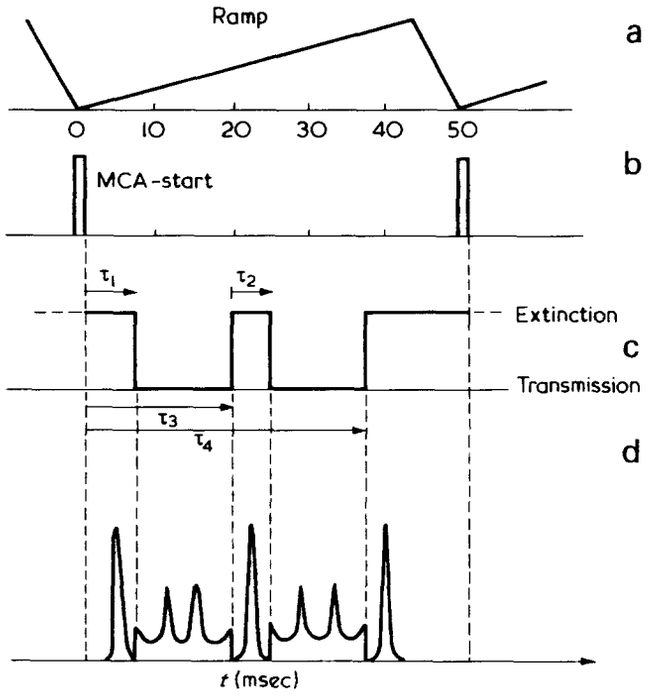

Figure 3 PC controlled Brillouin spectrum: (a) Ramp signal for FP; (b) MCA start pulse; (c) PC control signal Q with adjustable time constants $\tau_1 \ldots \tau_4$; (d) Brillouin spectrum modified by the PC (central peak extinction ratio 1:1000)

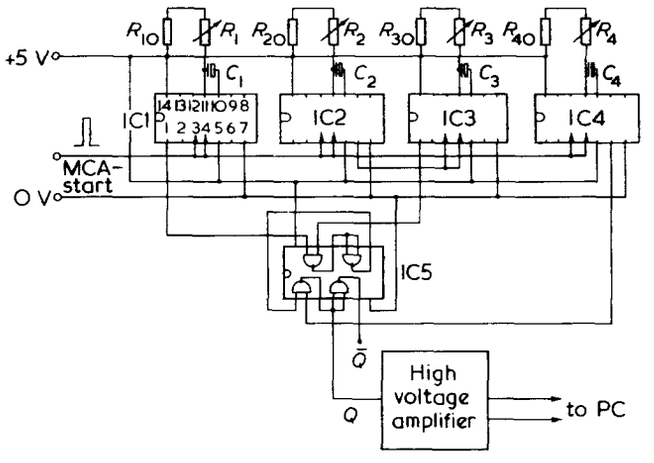

Figure 4 Circuit of the PC control pulse generator PG (as described in the text)

All time constants, the transmission and the extinction level can be adapted to the conditions given by the experiment. The transmission coefficient for the green argon line (514.5 nm) can be regulated between 90 and 0.1%; the rise time of the Pockels cell is about 10 nsec.

Furthermore the use of the PC allowed us to increase considerably the number of scans before reaching the counting capacity of the MCA.

The PC became indispensable when the sample tested was aligned in the 'anti-reflection' (*Figure 5b*) or in the 'reflection' position (*Figure 5c*) in which a large portion of the laser light reaches the pinhole of the photomultiplier directly.

If several spectral lines of a Brillouin spectrum appear within the free spectral range, it may be difficult to relate these spectral lines properly. This problem may be avoided by investigating the temperature dependence of the Brillouin lineshift and by changing the free spectral range of the FP.

In our measurements of the temperature dependence we used two different cryostats. Between 173K and 373K we used a cryostat made in our laboratories and below 173K an Oxford cryostat (CF 204). Both cryostats could be temperature-stabilized to about 0.1K. Temperatures were measured either by a resistance thermometer Pt100 or by a thermocouple.

Figures 5a–5e show the scattering geometries used for most of our experiments. Most of the samples investigated were in the form of flat cubes (see *Table 1*). The choice of the coordinate axis relative to the samples (*Figure 5*, encircled numbers) is somewhat arbitrary. However, the coordinate ① is always in the direction of sample thickness. For the film samples 4–7 axis ② is always in the film plane, but normal to the roll direction. For the melt flow-injection samples (1–3) axis ② always lies parallel to the melt flow direction. The scattering positions I and III in *Figures 5a–5c* indicate that the investigated volume elements are very close to the surface of the sample. If there is any change of structure between bulk (II) and surface (I, III) material, we can hope to discover this difference in structure by BS.

Provided that the outer scattering angle equals 90° in *Figure 5c*, the inner scattering angle θ_i is greater than 90°; in the case of *Figure 5b* the inner scattering angle θ_i is smaller than 90° when the sample is surrounded by air. The latter case is of special interest, because the equation for the sound velocity (equation 1): transforms using Snellius' refraction law to equation (2):

$$v = \frac{f_\Omega \lambda_\omega}{2 n_i \sin \dfrac{\theta_i}{2}} \tag{1}$$

where f_Ω is the hypersonic frequency; n_i is the refractive index of the sample for the appropriate polarization of the light; θ_i is the scattering angle in the sample and λ_ω vacuum laser wavelength.

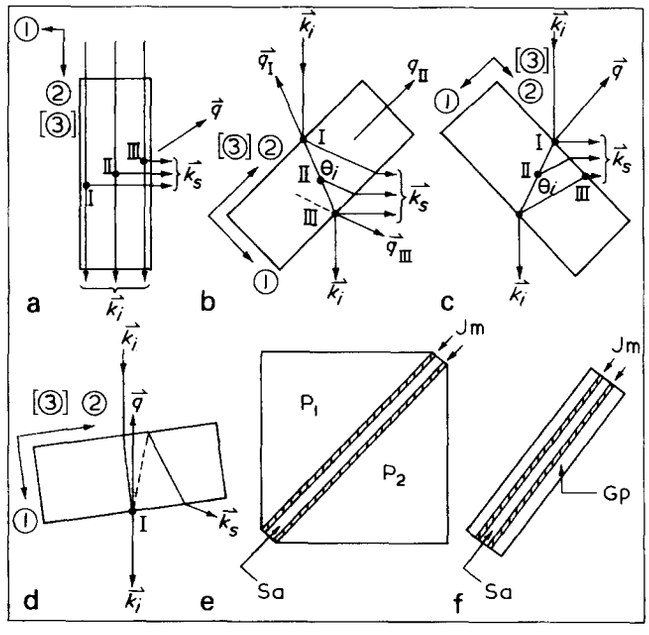

Figure 5 The different scattering geometries used: ①, ②, ③, Coordinate direction; k_i, k_s wavevector of incident and scattered light; q phonon wavevector; I, II, III Scattering positions; P1, P2 prisms; Sa, sample; Im,immersion; GP, glass plate

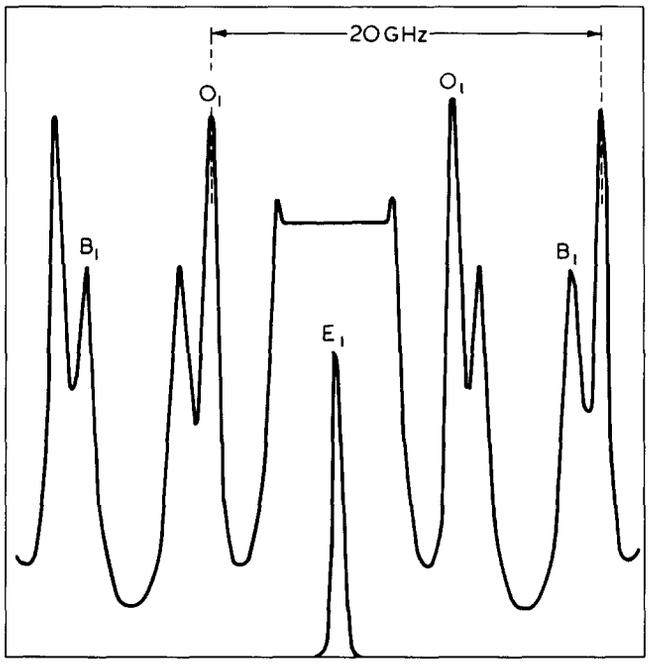

Figure 6 Brillouin spectrum from the 'antireflection' scattering geometry. E_1 Rayleigh line; O_1, B_1 to E_1 corresponding Brillouin lines due to ordinary and back scattering processes, respectively (see *Figure 5b*)

$$V = \frac{f_\Omega \lambda_\omega}{2 n_a \sin \frac{\theta_a}{2}} \qquad (2)$$

where n_a is the outer refractive index and θ_a is the outer scattering angle. Therefore, if the sample just bisects the outer scattering angle as in *Figure 5b* the measured Brillouin shift does not depend on the refractive index of the sample for arbitrary θ_a. This especially important in measurements of the temperature dependence of the hypersonic velocity, because there is no need to know the temperature dependence of n_i.

If the sample under test is isotropic and furthermore, if there is no dispersion, we can use the scattering geometries of *Figures 5a* and *5b* with equations (1) and (2) to determine the approximate temperature dependence of the refractive index (see below).

Another feature of the scattering geometry in *Figure 5b* is the fact that in the scattering positions I and III one obtains 'phonon lines' in the spectrum not only corresponding to wavevector q_{II} but also for the wavevectors q_I or q_{III}, respectively (*Figure 6*). The detection of the q_I and q_{III} phonon is indirect because we need the surface I or III as a reflection surface. Fortunately, the transmission losses at these surfaces are compensated by the increased scattering volume (depending on the sample thickness) in the back-scattering situation. As we will see in the next section, there was practically no difference of intensity between q_I, q_{II} and q_{III} phonon lines (*Figure 6*). However, typical surface effects may be obscured when the scattering volume is large. However, for the scattering geometry shown in *Figure 5d* the advantage of the large intensity for the back-scattering is lost and the scattering intensity is mainly determined by Fresnel's diffraction laws. In certain cases the scattering geometry given by *Figure 5d* may also be of interest because we can measure the line-shift of two different phonon wavevectors (relative to the sample geometry) in one scattering geometry by a slight shift of lens L_2 (see *Figure 2*).

The measurements on the film samples 4–7 have been made exclusively in the scattering geometries given by *Figures 5b* and *5c*. To stabilize the film samples mechanically we put the samples either between two glass plates or two prisms (*Figures 5c* and *5f*). As bonding material we used different immersion liquids of appropriate refractive indices such as immersion oil (Merck), Canada balsam or water-glass. The spectra were not altered by the different immersion liquids, so we could exclude the influence of the immersion substances on the hypersonic behaviour of the samples, e.g. due to swelling. However, we preferred the use of water-glass as immersion liquid because it exhibits a less strong scattering compared with the other two substances. This is an important point in the investigation of very thin films such as the 18 μm film because we can never exclude completely the adjacent immersion liquid from the scattering volume.

RESULTS AND DISCUSSION

In the section above we have shown scattering geometries required to determine easily the complete set of elastic constants for polymeric materials using a flat sample. Only the two large surfaces should be optically polished. A convenient simplification for the elastic characterization is obtained using the scattering situations given in *Figures 5b*I or *5b*III because we investigate simultaneously phonon waves of differently directed wavevectors relative to the sample geometry. These situations (I, III) are obtained simply by a small horizontal shift of lens L_2 (*Figure 2*). For thin samples (<4 mm) the scattering angle is only weakly affected. Clearly these scattering situations are particularly useful at temperatures at which a fast change or reorientation of the sample is impossible.

It may be pointed out that BS may be a sensitive experimental technique to study layer structures in polymers.

Figure 7 shows the hypersonic velocity for the well-annealed bulk material (sample 8) and the thickness-dependent sound velocity of the films (samples 4–7) for different orientations of the phonon vector relative to the film. The sound velocity of the bulk sample 8 is

$$v_{90N,II}^{309} (1\,1\,0) = 2265 \text{ m/sec}$$

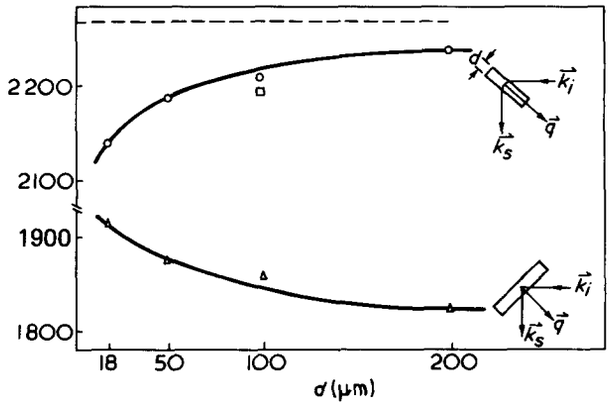

Figure 7 Sound velocity v in P4MP1 as a function of film thickness d for three different orientations of the phonon wavevector relative to the film plane and the roll direction, which is parallel to coordinate direction ③. The broken line indicates the sound velocity of the annealed bulk sample 8

and is always greater than any sound velocity measured in the films for the nomenclature (see *Table 2*). This may be understood from the fact that the crystallinity of the bulk material amounts to 32% whereas the crystallinity of the films is not higher than 27% (see *Table 1*). The strong influence of the crystallinity on the elastic behaviour of polymers has been demonstrated, e.g. by Leitner[10], for natural rubber at 273K.

We know from X-ray measurements that our P4MP1 films exhibit a planar crystallite orientation superposed by a small uniaxial orientation. From our BS measurements (*Figure 7*) we deduce an anisotropy of the sound velocity of the 200 μm film of 19% which reduces to 10% in the case of the 18 μm film. The upper curve of *Figure 7* represents the thickness dependence of the sound velocity parallel to the film plane but normal to the roll-direction. The lower curve of *Figure 7* represents the thickness dependence of the sound velocity for a phonon orthogonal to the film plane. For the 100 μm film we have also investigated the sonic anisotropy within the film plane which does not exceed the accuracy of the measurements.

In order to understand this behaviour, measurements on thicker samples (samples 1–3) just above the glass transition temperature were performed to study dispersion, anisotropy and surface effects. Additionally, we present the sonic velocity and an estimation of the index of refraction as a function of temperature. We shall first discuss anisotropy effects in the bulk (as opposed to the surface) of the samples 1–3 and 8.

The well-annealed sample 8 showed no elastic anisotropy as was demonstrated previously[3]. Samples 1–3 were cut from different corners of an injection-moulded sheet of P4MP1 (see above). *Table 2* shows that there is no anisotropy within the error of measurement (1%) for the bulk sound velocity of sample 1. For this sample we deduce, therefore, a medium bulk sound velocity of 2186 ± 20 m/sec at 309K which is about 3.5% smaller than that of sample 8 (see *Figure 7*). Sample 3 has not been investigated from the point of view of anisotropy but probably behaves in a similar way to sample 2. From *Table 2*, lines 1 8 and 12, we deduce that at 309K the largest sound velocity is observed in the (1 1 0) direction. This means that the appropriate phonon vector makes an angle of 45° with the plane of the surface. The smallest sound velocity is found in the (1 0 0) direction,

Table 2 Hypersonic velocities, v, and corresponding frequencies, f, for different scattering geometries and samples: $v = v^{T,W}_{\theta X,Y}$, T temperature in (K); W polarization of the incident laser beam and the scattered light relative to the scattering plane (Va vertical polarized input – no polarization output, VV vertical-vertical, VH vertical-horizontal), θ outer scattering angle, X scattering geometry ($X = N$ means normal and corresponds to *Figure 5a*, $X = A$ means antireflection corresponding to *Figure 5b*, $X = R$ means reflection corresponding to *Figure 5c*), Y specification of the scattering volume relative to the sample (I, II, III see *Figures 5a–5c*), (a, b, c) arbitrary vector (referred to the coordinate system of the sample) parallel to the phonon wavevector. *n*, no measurement; *np*, no phonon identified

No.	Hypersonic velocity (m/sec); corresponding frequency (GHz)	Sample 1		2	3	No.	Hypersonic velocity (m/sec); corresponding frequency (GHz)	Sample 1	2	3
1	$v^{309,Va}_{90N,II}(-1\ -1\ 0)$	*n*		2322	*n*	14	$v^{309,VV}_{90A,I}(0\ 1\ 0)$	2200	*n*	⟨2235⟩
	f			9.39			*f*	6.05		⟨6.14⟩
2	$v^{309,VV}_{90N,II}(-1\ -1\ 0)$	⟨2181⟩		*n*	*n*	15	$v^{309,VH}_{90A,I}(0\ 1\ 0)$	*np*	*n*	*np*
	f	⟨8.82⟩					*f*			
3	$v^{309,VH}_{90N,II}(-1\ -1\ 0)$	*np*		*np*	*n*	16	$v^{309,Va}_{90A,III}(0\ 1\ 0)$	2223	*n*	2267
	f						*f*	6.11		6.23
4	$v^{309,Va}_{90N/I}$	2267	1134	*n*	*n*	17	$v^{309,Va}_{90A,I}(X\ Y\ 0)$	2136	*n*	⟨2167⟩
	f	9.17	4.58				*f*	12.22		⟨1239⟩
5	$v^{309,VV}_{90N,III}(-1\ -1\ 0)$	2203	1114	*n*	*n*	18	$v^{309,VH}_{90A,I}(X\ Y\ 0)$	*np*	*n*	*np*
	f	8.91	4.50				*f*			
6	$v^{309,VH}_{90N,III}(-1\ -1\ 0)$		1055	*n*	*n*	19	$v^{309,Va}_{90A,III}(U\ V\ 0)$	2125	*n*	2187
	f		4.27				*f*	12.15		12.50
7	$v^{309,Va}_{90N,III}(-1\ -1\ 0)$	⟨2187⟩		*n*	*n*	20	$v^{309,Va}_{90A,II}(0\ 10)$ in immersion	2199	*n*	*n*
	f	⟨8.84⟩					*f*	9.16		
8	$v^{309,Va}_{90R,II}(-1\ 0\ 0)$	2174		2153	*n*	21	$v^{309,Va}_{90A,II}(0\ 0\ 1)$	2187	*n*	*n*
	f	10.90		10.79			*f*	6.02		
9	$v^{309,VH}_{90R,II}(-1\ 0\ 0)$	*np*		*np*	*n*	22	$v^{309,Va}_{90A,I}(0\ 0\ 1)$	2112	*n*	*n*
	f						*f*	5.81		
10	$v^{309,Va}_{90R,I}(-1\ 0\ 0)$	2109		*n*	*n*	23	$v^{190,Va}_{90N,II}(-1\ -1\ 0)$	*n*	2638	*n*
	f	10.57					*f*		10.67	
11	$v^{309,VH}_{90R,I}(-1\ 0\ 0)$	*np*		*np*	*n*	24	$v^{243,Va}_{90N,I}$	1215	*n*	*n*
	f						*f*	4.91		
12	$v^{309,Va}_{90A,II}(0\ 1\ 0)$	2189		⟨2230⟩	⟨2225⟩	25	$v^{190,Va}_{90R,II}(-1\ 0\ 0)$	*n*	2465	*n*
	f	6.02		⟨6.13⟩	⟨6.11⟩		*f*		12.37	
13	$v^{309,VH}_{90A,II}(0\ 1\ 0)$	*np*		*np*	*np*	26	$v^{190,Va}_{90A,II}(0\ 1\ 0)$	2568	2538	*n*
	f						*f*	7.06	6.97	

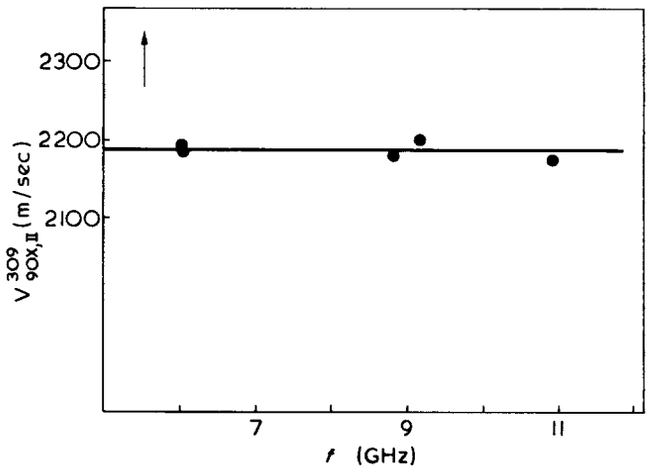

Figure 8 Dispersion behaviour for the bulk phonon sound velocity v in P4MP1

normal to the plane of the film. As will be discussed later, the anisotropy of the sound velocity of sample 2 may not be correlated with dispersion effects. The difference between the largest and the smallest sound velocities of sample 2 is about 8%. A comparison of the three different bulk sound velocities in sample 2 with those of sample 1 (ν_{iso}) yields:

$$\frac{\nu(1\,1\,0) - \nu_{iso}}{\nu_{iso}} \hat{=} 6.2\%$$

$$\frac{\nu(1\,0\,0) - \nu_{iso}}{\nu_{iso}} \hat{=} -1.5\%$$

$$\frac{\nu(0\,1\,0) - \nu_{iso}}{\nu_{iso}} \hat{=} 2.0\%$$

This anisotropy seems to be due to sample preparation (melt flow) and is predominantly related to the amorphous part of the material because the effect can be reduced by annealing at 360K.

As the polarization vectors of the incident and the scattered light remain fixed relative to the indicatrix of sample 2 for the three discussed scattering geometries, the refractive index cannot influence this anisotropy.

From *Figure 9*, the glass transition temperature is determined to be 288K. The glass transition is indicated by a change in the inclination of the sound velocity–temperature curve. The change of inclination does not follow directly from a relaxation process (because the Brillouin frequencies are well above all relaxation processes for P4MP1 connected with the glass transition) but is due to a spontaneous change in free volume at the transition temperature[17]. BS measurements seem to give the 'transition temperature' rather more accurately than classical methods such as d.s.c.

The accuracy of the temperature-dependent elastic constants determined by BS is often limited by the fact that neither the temperature-dependent refractive index nor the temperature-dependent density are known. Using the scattering geometries of *Figures 5a, 5b* and *5c* we are able to determine the refractive index within the accuracy of the Brillouin experiment. Such an estimation will now be made from P4MP1 at 190K. At 190K we find from *Table 2*, lines 23, 25 and 26 that the anisotropy of the bulk velocity of sample 2 has approximately the same value as at 309K. The discrepancy, smaller than 0.7%, is within the accuracy of measurement. In order to calculate the sound velocities from lines 23, 25 and 26 we have used the refractive index at room temperature. As lines 2, 8, 12, 20 and 21 of *Table 2* and *Figure 8* indicate, there is no dispersion at all in P4MP1 at 309K. The hypersonic frequencies vary for these spectra between 6 and 11 GHz. From *Figure 9* it is clear that dispersion effects may be neglected at temperatures between T_g and 17K. If it is assumed that the refractive indices at 309 and 190K are identical, the same hypersonic anisotropy is obtained at both temperatures. We believe that there is no reason for a drastic change of the elastic anisotropy on changing the temperature. If we accept this, the refractive index may have changed less than 1% (this is the uncertainty in the sound velocities) between 309 and 190K. This would result in a temperature coefficient of the refractive index of 10^{-4} K^{-1} or less.

Our measurements on injection-moulded P4MP1 suggest that the surface exhibits a different elastic behaviour from the bulk (see *Table 2*) *Figure 10* shows a typical spectrum measured close to the surface of such an injection-moulded sample for a phonon wavevector in the (1 1 0) direction.

Figure 10 contains an *VV*-polarized spectrum with a quasilongitudinal and quasitransverse phonon. Likewise, we have observed the very weak pure transverse phonon in *VH* scattering (see *Table 2*). A special surface structure coming from transcrystallization is not unexpected for melt-injected polymer samples[11,12]. From our BS measurements we infer, for our injection-moulded samples, a macroscopic weak orthorhombic (nearly tetragonal) symmetry for the elastic behaviour at the surfaces. It follows from *Table 2* that there is only a small anisotropy of the sound velocity of the longitudinal phonons at the surfaces. We should like to emphasize that for the (1 0 0) and the (0 0 1) direction there

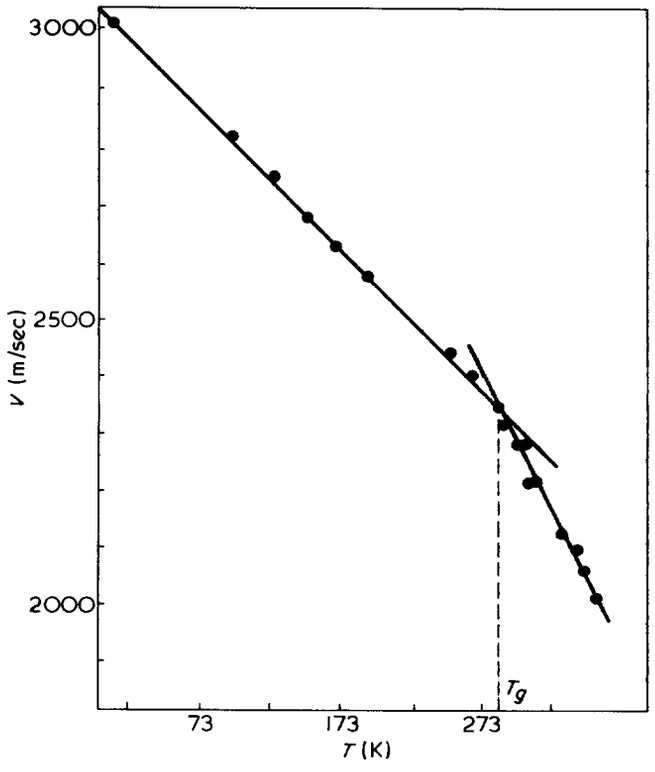

Figure 9 Phonon sound velocity v in P4MP1 in the bulk *versus* temperature. Glass transition temperature T_g = 288K

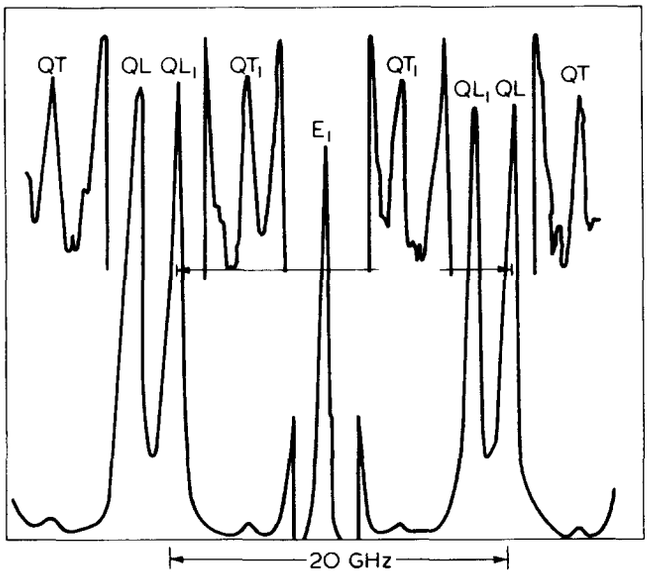

Figure 10 Brillouin spectrum for the (309, *VV* 90,I) scattering geometry. E_1 Rayleigh line QT_1 Brillouin line for the quasitransverse phonon, QL_1 Brillouin line for the quasilongitudinal phonon, both corresponding to the Rayleigh line E_1. Free spectral range 20 GHz

is no difference between the sound velocities, whereas the sound velocity in the (010) direction is about 5% higher. All detected quasi- and pure phonons are well-polarized. In the case of *VH* polarization there was no hint of quasi-phonons at all.

We have not observed transverse phonons in either of the coordinate directions. However, they could be obscured by the Rayleigh wing which is always very strong for the scattering positions I and III in *Figures 5b* and *5c*. One should remember that the Pockels cell cannot increase the resolving power of the interferometer system as an iodine filter at 514.5 nm or a higher contrast factor of the FP can. However, the use of iodine filters has the disadvantage of line deformation. The absence of any quasitransverse phonon for the positions I and III may be a hint that the somewhat arbitrary coordinate systems are parallel to the internal 'physical' coordinate system in the surface.

It is uncertain why, for the scattering geometry $^{309\,VH}_{90N,II}$ (1 1 0), even after counting for several hours we did not detect any transverse phonon. (In the isotropic bulk one should expect one degenerate transverse phonon.) From the fact that such a phonon has been seen in the surface layer one may conclude that the surface structure increases the scattering cross-section in a certain manner for the tranverse phonon. However this remains an open question.

We are able to give some matrix elements of the elastic matrix for the surface of sample 1 (orthorhombic symmetry). With a density of $\rho = 0.835$ g/cm^3 [10] we can calculate c_{11}, c_{22} and c_{33} directly with $c = \rho v^2$:

$$c_{11}^{309} = 3.71 \times 10^9 \text{ N/m}^2$$

$$c_{22}^{309} = 4.08 \times 10^9 \text{ N/m}^2$$

$$c_{33}^{309} = 3.72 \times 10^9 \text{ N/m}^2$$

The surface elastic constant for the melt flow direction (c_{22}) differs by 10% from the two other coordinate directions. This probably follows from a small uniaxial orientation of the crystallites in the surface because this effect could not be caused by annealing in contrast to a similar effect in the bulk.

The elastic constant of the isotropic bulk for the same sample is:

$$c_{11}^{309} = c_{22}^{309} = c_{33}^{309} = 3.99 \times 10^9 \text{ N/m}^2$$

The last value lies between the two for the surface layer. From Christoffel's equation (see, for example, ref 13) one deduces two relations for calculating c_{12} and c_{66}.

$$c_{66} = c_Q + c_{QT} - \frac{1}{2}[c_{11} + c_{22}] \quad (3)$$

$$c_{12} = \frac{1}{2}\left(4(c_{QL} - c_{QT})^2 - (c_{11} - c_{22})^2\right)^{1/2} - c_{66} \quad (4)$$

c_{QL} and c_{QT} are determined from *Table 2*, lines 4 and 5: $c_{QL}^{309} = 4.17 \times 10^9$ N/m^2; $c_{QT}^{309} = 1.05 \times 10^9$ N/m^2. With these values and the values for c_{11} and c_{22} we calculate using equations (3) and (4): $c_{66}^{309} = 1.33 \times 10^9$ N/m^2; $c_{12}^{309} = 1.79 \times 10^9$ N/m^2. From the *VH* scattering results (*Table 2*, line 6) we only can calculate an average value of c_{44} and c_{55}:

$$c_T^{309} = (c_{44} + c_{55})/2 = 0.93 \times 10^9 \text{N/m}^2$$

At present we have no information on c_{13} and c_{23}. The calculated elastic constants of the bulk and the surface layer of P4MP1 are one order of magnitude smaller than those of typical dielectric crystals at room temperature (such as ammonium sulphate[14] or potassium selenate[15]), which seems to be very reasonable.

We now go back to the beginning of this section to discuss again the thickness dependence of the sound velocity of different P4MP1 films (*Figure 7*). We must give an explanation as to why the thinner films seem to be elastically more isotropic than the thicker ones. Suppose that each film has a sandwich structure, consisting of two surface layers and the bulk (*Figure 12*). Suppose further that the surface layer behaves similarly as in the case of sample 1; hence we predict a weak orthorhombic symmetry. Furthermore, we predict a nearly planar orientation of the chain molecules for the bulk of the films. If the oriented bulk had a larger sound velocity in the film plane compared with that of the surface and if the bulk sound velocity normal to the film plane were less than that of the surface we expect the behaviour seen in *Figure 7*.

This may be only one of the possible explanations, because of the large number of uncontrollable parameters involved (e.g. crystal size contribution, orientation correla-

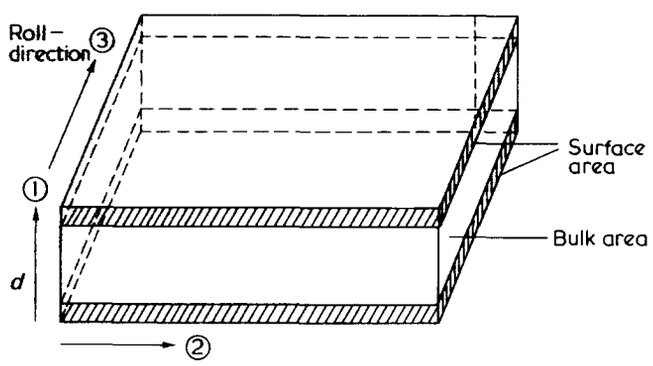

Figure 11 Supposed layer structure of the film samples of thickness *d*

tion, continuity etc.). However, from these results we conclude that there may be a very different elastic behaviour between the surface and the bulk of polymer samples. Therefore, one should be cautious in deducing bulk properties from film measurements.

For technical reasons we have restricted our measurements to the temperature range 17 to 353K, and to the sound velocity, without discussing attenuation. Measurements in the temperature range 4 to 600K are still in progress.

For the attenuation measurements we are going to combine the normal BS with the technique of microwave-induced phonons, developed in our Institute[16]. On the one hand this method will increase the scattering efficiency and on the other it will enable us to deduce the hypersonic attenuation without discussing the Brillouin linewidth.

ACKNOWLEDGEMENT

The authors acknowledge very fruitful discussions with Professor Unruh and Professor Gleiter. Thanks are due to Dr Heise for the X-ray measurements and to the chief of our workshop, E. Meyer, for building many parts of our Brillouin set-up.

REFERENCES

1 Saunders, *J. Polym. Sci. (B)* 1964, **2**, 755
2 Sandercock, J. R. *Phys. Rev. Lett.* 1972, **29**, 1735
3 Krüger, J. K., Sailer, E., Spiegel, R. and Unruh, H. -G. *Prog. Colloid Polym. Sci.* 1978, **64**, 208
4 Patterson. G. D. *J. Polym. Sci.* 1976, **14**, 143
5 Patterson, G. D. *J. Polym. Sci.* 1976, **14**, 1909
6 Wunderlich, B., Jain, P. C. and Chaubey. D. R. *J. Polym. Sci. (Polym. Phys. Edn)* 1977, **15**, 2271
7 Mitsui Petrochem. Ind. Ltd. Technical report
8 'Polymer Handbook (Eds J. Brandrup and E. H. Immergut) 2nd Edn, Wiley, New York, III 144
9 Spiegel, R. Staatsexamensarbeit, Saarbrücken, 1977
10 Leitner, M. *Trans. Faraday Soc.* 1955, **51**, 1015
11 Lovering, E. G. *J. Polym. Sci. (A-2)* 1970, **8**, 1697
12 Kautz. M. R., Newmann, H. D. and Stigale, F. H. *J. Appl. Polym. Sci.* 1972, **16**, 1249
13 Auld, B. 'Acoustic Fields and Waves in Solids I', Wiley, New York, 1973, p 210
14 Unruh, H. -G., Krüger, J. and Sailer, E. *Ferroelectrics* 1978 in press
15 Krüger. J. and Unruh, H. -G. in preparation
16 Krüger, J. and Unruh, H.-G. *Solid State Commun.* 1977, **21** 583
17 Brody, E. M., Lubell, G. J. and Beatty, C. L. *J. Polym. Sci. (Polym. Phys. Edn)* 1975, **13**, 295